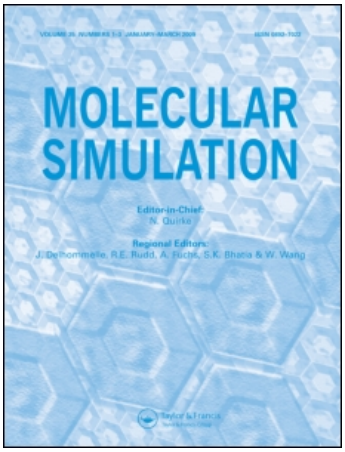

Molecular Simulation
Publication details, including instructions for authors and subscription information:
http://www.informaworld.com/smpp/title~content=t713644482

An Ion Conducted Tour through $LaMO_3$ Perovskite-based Oxide Materials

M. Saiful Islam[a]
[a] Department of Chemistry, University of Surrey, Guildford, UK

To cite this Article Islam, M. Saiful(1998) 'An Ion Conducted Tour through $LaMO_3$ Perovskite-based Oxide Materials', Molecular Simulation, 21: 2, 127 — 141
To link to this Article: DOI: 10.1080/08927029808022055
URL: http://dx.doi.org/10.1080/08927029808022055

Molecular Simulation, 1998, Vol. 21, pp. 127–141
Reprints available directly from the publisher
Photocopying permitted by license only

AN ION CONDUCTED TOUR THROUGH $LaMO_3$ PEROVSKITE-BASED OXIDE MATERIALS

M. SAIFUL ISLAM

Department of Chemistry, University of Surrey, Guildford GU2 5XH, UK

(Received October 1997; accepted January 1998)

This paper will review recent atomistic simulations of the oxygen ion transport and defect properties of the $LaMO_3$(M = Mn, Co, Ga) perovskite-structured materials. Both static lattice and molecular dynamics techniques are used which have been applied previously to a rich variety of ceramic oxides. The mechanistic features and energetics of oxygen vacancy migration are examined in relation to ion size factors and lattice relaxation. The oxidation reaction in doped $LaMO_3$ involving the creation of hole species from oxygen vacancies is also considered. Finally, MD simulations are used to yield information on oxygen diffusion coefficients and ion trajectories in the $La_{1-x}Sr_xMnO_3$ system.

Keywords: Perovskite; oxygen diffusion; $LaMO_3$

1. INTRODUCTION

The search for oxide materials with high oxygen ion conductivity has attracted much attention owing to both the technological applications (*e.g.*, fuel cells, air separation membranes) and the fundamental interest of high ionic mobility in inorganic solids [1, 2]. Due to the elevated temperatures required to sustain adequate oxygen ion conductivity in current materials there is considerable interest in developing new ceramic oxides with high conductivity at lower operating temperatures.

The perovskite-structured oxides based on $LaMO_3$ (where for example M = Mn, Co, Ga) comprise a rich family of compounds that have potential applications in solid oxide fuel cells (SOFC) and heterogeneous catalysis; for instance, mixed-conducting Sr doped $LaMnO_3$ finds use as the cathode material in SOFCs [3], whereas doped $LaGaO_3$ shows superior oxygen ion

conductivity than the conventional Y/ZrO_2 electrolyte at lower operating temperatures [4]. In addition, there have been numerous studies on proton conducting perovskites, with most attention focused on $A^{2+}B^{4+}O_3$ materials (where A = Sr, Ba and B = Ce, Zr) [5].

These perovskite oxides are typically doped on the La site with low-valent cations which gives rise to the formation of mobile oxygen vacancies and/or electronic defects. Clearly, the role of defects and dopants, as well as the mechanisms of ion transport are crucial for the complete understanding of their behaviour. To shed light on these issues, computer modelling techniques have been applied to these oxides, which are now well established tools in probing materials properties at the atomic level. The reliability of such a modelling approach has been demonstrated by similar work on metal oxide catalysts [6, 7] and the perovskite-based cuprate superconductors [8, 9].

This article will highlight recent studies of the defect and oxygen transport properties of $LaMO_3$ perovskites using both static lattice and molecular dynamics (MD) techniques, with particular attention given to the $LaMnO_3$, $LaCoO_3$ and $LaGaO_3$ systems. Here we have explored the energetics and pathways for oxygen ion diffusion, as well as trends in migration energy with changes in cation size.

2. SIMULATION METHODS

The simulations are formulated within the framework of the Born model, the main features of which are the nature of the interatomic potentials and the modelling of perfect and defective lattices. The present account of these widely used techniques will be brief since comprehensive reviews are given elsewhere [10].

The effective potentials describing the interatomic forces are represented by ionic, pair-wise potentials of the form

$$\emptyset_{\alpha\beta}(r) = \frac{-Z_\alpha Z_\beta e^2}{\varepsilon r} + A_{\alpha\beta}\exp(-r/\rho_{\alpha\beta}) - C_{\alpha\beta}/r^6, \qquad (1)$$

which includes a long-range Coulombic interaction, and a short-range term to model the repulsions and van der Waals attractions between electron charge clouds. Because charge defects will polarise other ions in the lattice, ionic polarisibility must be incorporated into the potential model. The shell model provides a simple description of such effects and

has proven to be effective in simulating the dielectric properties of ceramic oxides.

An important feature of these calculations is the treatment of lattice relaxation about the point defect or migrating ion. The Mott-Littleton approach is to partition the crystal lattice into two regions so that ions in a spherical inner region surrounding the defect are relaxed explicitly. In contrast, the remainder of the crystal, where the defect forces are relatively weak, is treated by more approximate quasi-continuum methods. In this way local relaxation is modelled effectively and the crystal is not considered simply as a rigid lattice through which ion species diffuse.

The potential parameters for the oxide systems were derived by empirical procedures using their observed perovskite structure (Fig. 1). For the $LaMO_3$ compounds considered, the potential parameters for the La—O and (O —O) interactions were derived simultaneously, resulting in a consistent set of potentials. Table I lists the interatomic potentials and shell model parameters used in this study.

The molecular dynamics (MD) technique consists of an explicit dynamical simulation of the ensemble of particles for which Newton's equations of motion are solved. Repetition of the integration algorithm yields a detailed picture of the evolution of the system as a function of time. This technique allows the inclusion of the kinetic energy for an ensemble of ions (to which periodic boundary conditions are applied) representing the system simulated.

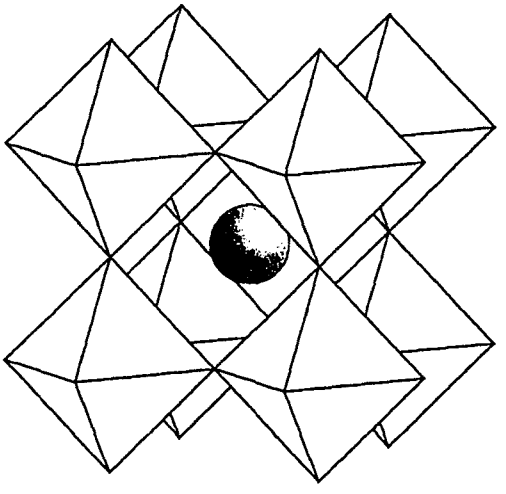

FIGURE 1 Cubic perovskite structure.

TABLE I Interatomic potentials for the $LaMO_3$ perovskites

Interaction	$A(eV)$	$\rho(\AA)$	$C(eV\AA^6)$	$Y(e)$	$k(eV\AA^{-2})$
La—O	1545.21	0.3590	0.0	−0.25	145.0
Mn—O	1267.5	0.3214	0.0	3.00	95.0
Co—O	1329.82	0.3087	0.0	2.04	196.3
Ga—O	2901.12	0.2742	0.0	3.00	99999
O —O	22764.3	0.1490	43.0	−2.24	42.0

The MD simulations reported here were performed using the DLPOLY code [11] with a simulation box comprising 2560 ions (*i.e.*, $8 \times 8 \times 8$ perovskite unit cells); the ensemble used imposes the conditions of constant temperature and pressure (NPT). The calculations were run using a time step (δt) of 10^{-15} s and for a total period of 50 ps including initial equilibration (of 4 ps). It is worth remarking that we are employing a longer time scale than the majority of previous MD simulations of polar solids. The doped system $La_{1-x}Sr_xMnO_3$ was modelled by the partial substitution of La by Sr (introduced at random) and the corresponding removal of oxygen ions as charge-compensating vacancy defects. The analysis of ion positions and velocities yields a wealth of dynamical detail: atomic diffusion coefficients may be obtained as may be mechanistic information by analysis of particle trajectories.

3. RESULTS AND DISCUSSION

3.1. Migration Mechanism and Ion Size Factors

Despite several reports on oxygen diffusion in $LaMO_3$ materials [12–23] the amount of information on fundamental mechanistic features is rather limited. We have investigated these problems by an extensive search of the potential energy surface for oxygen vacancy migration. The energy profiles are mapped out by calculating the defect energy of the migrating ion along the conduction path, and allowing relaxation of the lattice at each position. In this way the saddle-point configuration can be identified from which the energy barrier to migration is derived.

The resulting activation energies are reported in Table II together with the available values from experiment. Examination of the results confirms migration of oxygen ion vacancies as the lowest energy path. The calculated values accord well with the available experimental activation energies, although direct comparison is not straightforward since the observed values show significant variation. This scatter may reflect differences in experi-

TABLE II Calculated and experimental energies for oxygen ion migration

Compound	*Ecale (eV)*	*Eexpt (eV)*
$LaMnO_3$	0.86	0.73[a]
$LaCoO_3$	0.61	0.58[b] ; 0.78[c]
$LaGaO_3$	0.73	0.66[d] ; 0.79[e]

[a] Belzner [15]; [b] van Doorn [20]; [c] Ishigaki [12]; [d] Drennan [22]; [e] Ishihara [21].

mental conditions, doping levels and oxygen stoichiometry, as well as problems with phase purity. Nevertheless, we find, for example, that the calculated migration energy (0.73 eV) for $LaGaO_3$ is consistent with activation energies of 0.66 and 0.79 eV from dc conductivity [22] and SIMS studies [21] respectively. We should note that the calculated energies in Table II relate to intrinsic migration of oxygen defects and do not include energies of formation or association; these additional energy terms may account for the larger activation energies of about 1.9 eV that have been observed for the $La_{1-x}Sr_xFe_{1-y}Co_yO_{3-\delta}$ (LSFC) system [23].

In the saddle-point configuration, the migrating ion must pass through the opening of a triangle defined by two A site (La^{3+}) ions and one B site ion (Fig. 2). Clearly the repulsive interactions can be reduced by the outwards movement of the nearest cations. The simulation approach is able to model lattice relaxation and generate valuable information on local ion movements. It is worth recalling that ionic polarizability has been treated in our simulations by the shell model. Therefore, the crystal structure is not considered simply as a hard-sphere lattice with fixed ions. From our analysis we find average displacements of the La^{3+} and M^{3+} ions of 0.08Å and 0.07Å respectively, away from the mobile oxygen ion (shown in Fig. 2). These results emphasise that neglecting lattice relaxation effects at the saddle-point may be a serious flaw in previous ion size approaches based on a rigid hard-sphere model, in which the 'critical radius' of the opening is derived [24].

It is clear that the size balance between the A and B cations in the perovskite structure is an important factor for high ionic conductivity. A geometric analysis of the saddle-point configuration, as illustrated by Figure 2, has been employed before in the context of defining selection criteria for good ion conductors [24]. In addition, it is well established that simple geometrical limits for cation radii on the A and B sites can be defined by the so-called Goldschmidt Tolerance Factor given by:

$$t = (r_A + r_O)/\sqrt{2}(r_B + r_O) \quad (2)$$

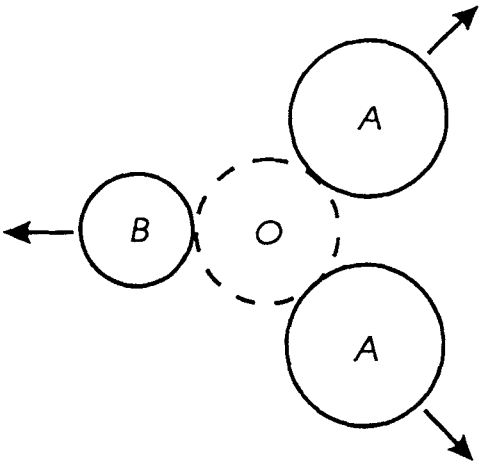

FIGURE 2 Saddle-point configuration for oxygen ion migration indicating cation relaxation.

where we note that, nominally, the perovskite structure is stable for $1.0 > t > 0.75$.

Here we examine further the relationship between migration energy and cation size within our simulation procedure. Our approach is to change systematically our interatomic potential model so as to calculate the vacancy migration energy as a direct function of the ionic size of the A and B cations. To assess these results, we consequently examined the relationship between the tolerance factor (t) and our calculated migration energies. The result is illustrated in Figure 3. Owing to the uncertainties of the ionic radii used, we must be cautions in giving detailed interpretations. Nevertheless, a degree of correlation exists between t and our calculated Emig with a clear minimum at about $t = 0.81$. Our calculations, therefore, suggest that materials with a t value of about 0.81 may lead to lower migration energies and faster diffusion, a result that may have practical consequences for fuel cells and oxidation catalysis.

We can attempt to rationalise these results in terms of lattice relaxation effects. As the mobile oxygen ion approaches the saddle-point it must pass through the centre of a triangle of cations (shown in Fig. 2). Our calculations have already shown that the repulsive overlap interactions can be reduced by the outwards relaxation of these cations. It appears, that the *minimum* in the tolerance factor corresponds to the most effective balance of the relaxation of the A and B cations at the saddle-point position. In other words, the even distribution of relaxation between the cations is an important factor for low energy barriers to oxygen ion migration.

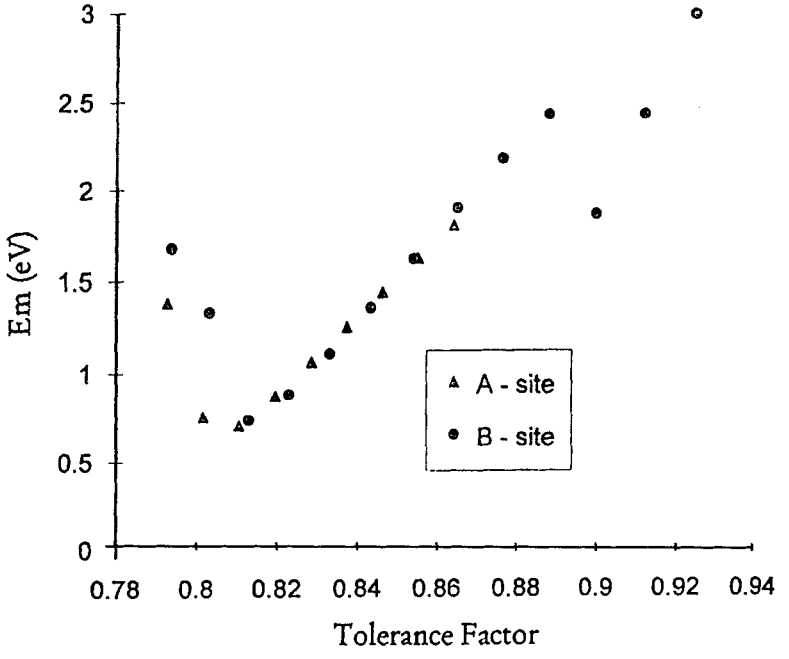

FIGURE 3 Calculated oxygen vacancy migration energy as a function of the perovskite tolerance factor (t).

3.2. Oxidation Reaction (Vacancy to Hole)

It is generally believed that the catalytic behaviour and the oxygen transport through fuel cell materials are partly controlled by the exchange between gas-phase oxygen and lattice oxygen of the doped $LaMO_3$ systems. In this context, we have considered the redox process involving the filling of oxygen vacancies by molecular oxygen to form electronic holes; such an oxidation reaction involves the dissociation of O_2 and can be written as

$$V_O^{\cdot\cdot} + \frac{1}{2}O_{2(g)} \rightarrow O_o^x + 2h^{\cdot} \tag{3}$$

where O_o^x is an oxygen anion on a normal site and $h^{\cdot}$ is a localised hole state. We note that the oxygen vacancies have already been introduced into the lattice by dopant (*e.g.*, Sr^{2+}) substitution. Our approach to electronic defects of $LaMO_3$ follows that used for simple binary oxides [6, 10] and for the cuprate superconductors [8, 9], in which we model the hole centres as M^{4+} and O^- substitutionals; the resulting hole energies are listed in Table IV. Our studies have favoured (on energetic grounds) M^{4+} holes in $LaMnO_3$

TABLE III Hole centre and oxidation energies (in eV)

(a) Hole centre *Compound*	M^{4+}	O^-
$LaMnO_3$	4.33	6.34
$LaCoO_3$	3.11	5.75
$LaGaO_3$	19.52	7.88
(b) Oxidation reaction (vacancy to hole) *Compound*	E_{ox}	
$LaMnO_3$	0.27	
$LaCoO_3$	−0.84	
$LaGaO_3$	3.78	

and $LaCoO_3$, but oxygen holes in $LaGaO_3$. Using these hole terms, the energies of the oxidation reaction (3) were calculated for all three systems and are also reported in Table IV.

The results indicate three main points. First, oxidation of doped $LaCoO_3$ is exothermic indicating a thermodynamically favourable reaction. While there is little quantitative data available for direct comparison, the calculated energetics are compatible with studies on nonstoichiometry and conductivity by Mizusaki *et al.* [13]. Thus, except at low oxygen partial pressures, we would expect holes (Co^{4+}) to predominate over vacancies and that oxidation will enhance the solubility of the dopant in the $LaCoO_3$ host. We note that experimental findings show mixed (electronic and ionic) conductivity in this material and that the *p*-type conductivity increases with increasing oxygen activity [13]. In addition, recent structural studies of $La_{1-x}Sr_xCoO_3$ ($x = 0.5$) have found evidence for ordering effects involving both Co^{4+} and oxygen vacancies [25]. Secondly, we calculate a small endothermic energy for $LaMnO_3$, thus significantly less favourable than that for $LaCoO_3$. These results are consistent with isotope experiments [14] which find a significant difference in oxygen exchange behaviour between $LaCoO_3$ and $LaMnO_3$. It has been noted previously by Steele *et al.* [1, 14] that a key factor is the relative "redox stability" of the transition metal cation occupying the B-site, where the stability of Mn^{3+} is greater than that of Co^{3+}. Our hole and oxidation energies are in accord with this trend in stability. Finally, in contrast to the systems containing transition metals, the oxidation reaction is highly unfavourable for doped $LaGaO_3$ indicating that ionic rather than electronic compensation (and hence ionic rather than electronic conductivity) predominates in this materials, as is observed [21, 22].

Our analysis has included all of the key terms in the oxidation process. There are, however, uncertainties in the absolute values due to the free-ion

energies employed. Nevertheless, our concern here is to understand the nature of the defect process responsible for the redox chemistry; for this task our modelling methods have proved to be reliable.

3.3. MD Simulations of Oxygen Ion Diffusion

We have already obtained *via* static lattice methods useful information on some of the factors controlling oxygen transport in $LaMO_3$ perovskites. Here we will amplify this knowledge by a detailed investigation of oxygen diffusion using Molecular Dynamics (MD) techniques which include thermal effects explicitly; these computational techniques have been successfully applied to a variety of ionic conductors, but have not been widely applied to perovskite type oxides. In the present work we have focused attention on the fuel cell material $La_{1-x}Sr_xMnO_3$, for which there is experimental diffusion data for direct comparison.

Atomic transport properties are extracted from the simulations using the time-dependent mean square displacements (MSD). The MSDs for all the ions in the doped system $La_{0.8}Sr_{0.2}MnO_3$ at 2000 K are presented in Figure 4. They clearly show that the MSD of the cations tends rapidly to a constant value following equilibration and confirms that there is no cation diffusion

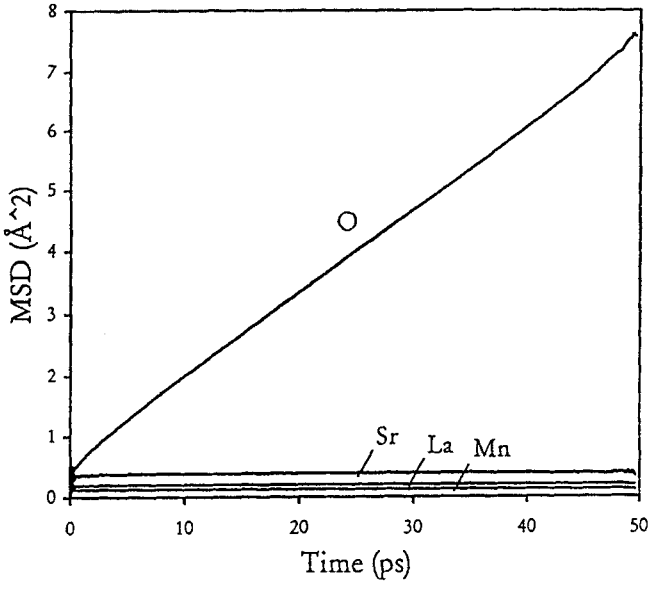

FIGURE 4 Mean square displacements of all the ions in $La_{0.8}Sr_{0.2}MnO_{3-y}$ at 2000 K.

in the perovskite oxide. However, the MSD for the oxygen ions increases with time indicating significant ion diffusion; this type of behaviour is found in simulations of other solid electrolytes such as Y/ZrO_2 [26]. We note that the basic features of the plots are very similar for all the temperatures considered between 800 and 2000 K.

The diffusion coefficient (D_i) can be obtained from the gradient of the plot of MSD against time according to the well known relation:

$$\langle r^2(t) \rangle = 6D_i t + B_i, \tag{4}$$

where B_i is the thermal factor arising from atomic vibrations. The calculated oxygen diffusion coefficients are presented in the form of an Arrhenius plot (In D *versus* $1/T$) in Figure 5, on which we also indicate experimentally determined values.

The results indicate that we have been able to calculate values of the oxygen diffusion coefficient (D_0) over a broad range of about two orders of magnitude, which is significantly wider than the experimental data. The diffusion coefficients for the manganate systems are in reasonable agreement with the available chemical diffusion coefficients of Belzner *et al.* [15]. From the slopes of the Arrhenius plots (Fig. 5) the activation energy for oxygen migration have been derived with values of 0.70 and 0.67 eV for $x = 0.2$ and 0.5 respectively. The slight curvature in the data points in Figure 5 is largely

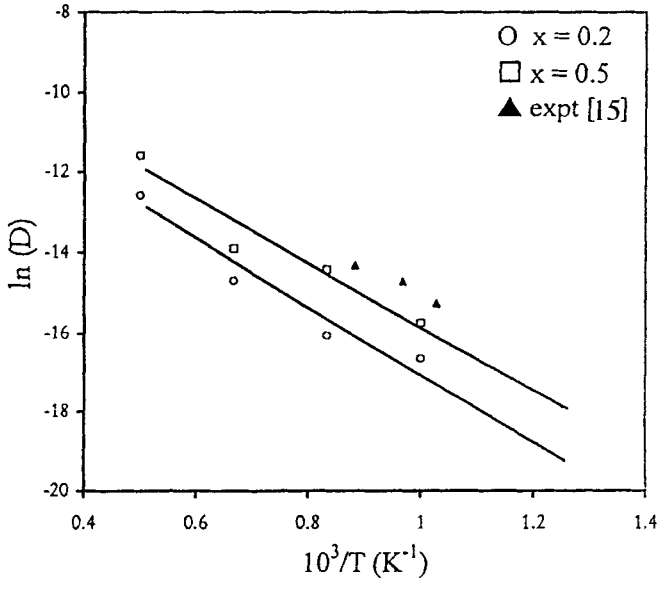

FIGURE 5 Arrhenius plot for oxygen diffusion in $La_{1-x}Sr_xMnO_{3-y}$.

due to the improved statistics of the simulations for the much higher diffusion coefficients at elevated temperatures. We have therefore neglected the point from the 800 K simulation, although the deviation at lower temperatures are within the uncertainties owing to the statistical errors of the data.

A major thrust of basic transport studies has been the determination of the atomistic mechanisms controlling bulk transport phenomena. Indeed, the unravelling of conduction pathways at the microscopic level, which can be difficult from purely experimental studies, is a powerful feature of the MD technique.

To gain further insight into the migration mechanism we have obtained "trajectory plots" which reveal the evolution of the displacement of the ions

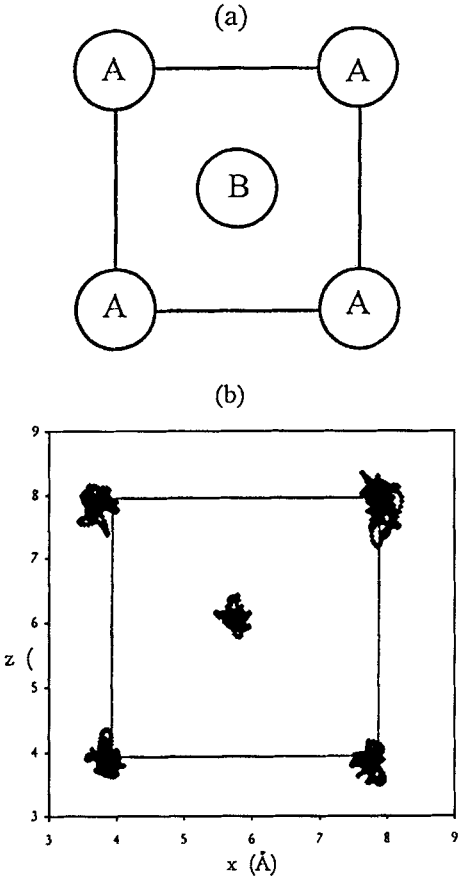

FIGURE 6 Trajectory plot of cations (a) schematic of cation positions in pefect laatice (b) $La_{0.8}Sr_{0.2}MnO_{3-y}$.

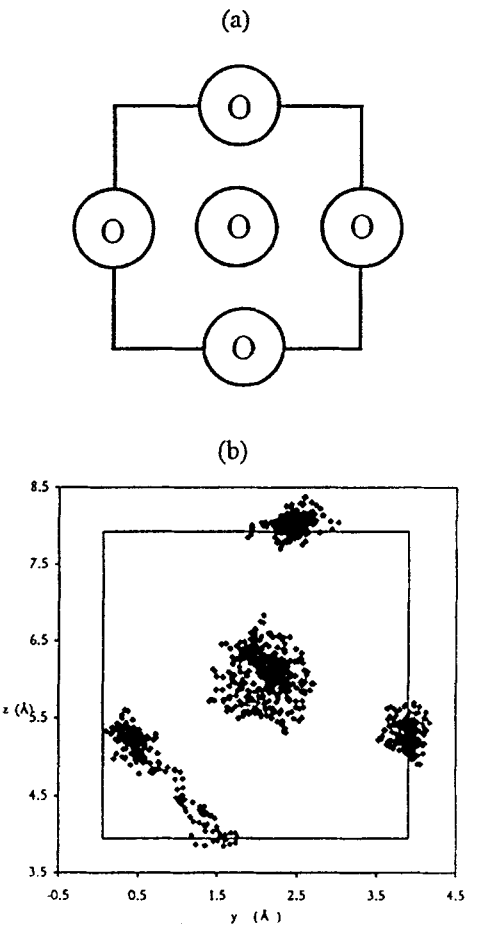

FIGURE 7 Trajectory plot of oxygen ions (b) schematic of an ion positions in perfect lattice (b) $La_{0.8}Sr_{0.2}MnO_{3-y}$.

(Figs. 6 and 7). It should be noted that these plots relate to a projection into the face of one unit cell (*i.e.*, the figures relate to ions in two layers parallel to the (100) plane). Figure 6 clearly indicates small vibrations of the cations about their lattice sites with no evidence of ion diffusion, which is typical behaviour for an ordered solid. In contrast, Figure 7 shows a more diffuse distribution on the oxygen sublattice for $La_{0.8}Sr_{0.2}MnO_3$ indicating significant ion motion: the diffusion of oxygen is illustrated by the spread of points between adjacent lattice sites along the octahedron edge. It is also apparent that the oxygen vacancies induce a strong relaxation of neighbouring anions causing a distortion of the octahedra.

Such rapid oxygen transport in these perovskite-type oxides is a vital characteristic for their application in solid oxide fuel cells, oxidation catalysis, and gas separation. However, we recognise that $LaMO_3$ materials show complex behaviour when acceptor doped because of the ability of the M cation to change valence which may lead to compensation by a mixture of oxygen vacancies and holes [1, 14]. Current MD studies are extending this work to include doped systems with a mixture of oxygen vacancy and hole compensation.

4. CONCLUSION

Atomistic computer simulations have been able to provide a deeper insight as to the fundamental defect and ion transport properties of the $LaMO_3$ (M = Mn, Co, Ga) perovskite oxides, which are relevant to their use in solid oxide fuel cells and other similar electrochemical applications.

Three main points have emerged from our discussion. First, a strong relationship between the calculated energy for oxygen vacancy migration and the perovskite tolerance factor is established. The simulations demonstrate the importance of lattice relaxation around the migrating ion, effects of which were neglected by previous ion size models based on a simple hard-sphere approach. Second, the energies of oxidation to form hole species predict the relative redox stability as: $LaCoO_3 < LaMnO_3 \ll LaGaO_3$; this is compatible with observation that find mixed ionic/electronic conductivity in doped $LaCoO_3$ but purely oxygen ion conductivity in doped $LaGaO_3$. Finally, oxygen diffusion coefficients for $La_{1-x}Sr_xMnO_3$ have been derived over a wider temperature range than the available experimental data. Analysis of the ion trajectories points to a conventional hopping mechanism along the MO_6 octahedron edge, with no evidence of correlated motion.

This work is being extended to encompass computational studies of surface oxygen exchange and proton transport in perovskite oxides, and of oxygen ion diffusion in related brownmillerite and Aurivillius phases.

Acknowledgements

The author is grateful to C. R. A. Catlow, M. Cherry and M. S. Khan for useful discussions. This work was supported by the EPSRC, BP Research and BG Gas Research and Technology.

References

[1] Steele, B. C. H. (1992). "Oxygen ion conductors and their technological applications" In: Solid State Ionics, Eds., Balkanski, M., Takahashi T. and Tuller, H. L., Elsevier, Amsterdam.

[2] Kendall, K. R., Navas, C., Thomas, J. K. and zur Loye, H. C. (1995). "Recent developments in perovskite-based oxide ion conductors", *Solid State Ionics*, **82**, 215.

[3] Minh, N. Q. (1993). "Ceramic fuel cells", *J. Am. Ceramic Soc.*, **76**, 563.

[4] Ishihara, T., Matsuda, H. and Takita, Y. (1994). "Doped $LaGaO_3$ perovskite-type oxide as a new oxide ionic conductor", *J. Am. Chem. Soc.*, **116**, 3801.

[5] Kreur, K. D. (1997). "On the development of proton conducting materials for technological applications", *Solid State Ionics*, **97**, 1.

[6] Islam, M. S., Ilett, D. J. and Parker, S. C. (1994). "Surface structures and oxygen hole formation on the La_2O_3 catalyst – a computer simulation study", *J. Phys. Chem.*, **98**, 9637.

[7] Balducci, G., Kaspar, J., Fornasiero, P., Graziani, M., Islam, M. S. and Gale, J. D. (1997). "Computer simulation studies of bulk reduction and oxygen migration in CeO_2-ZrO_2 solid solutions", *J. Phys. Chem.*, **101**, 1750.

[8] Islam, M. S., Read, M. S. D. and D'Arco, S. (1997). "From oxides to oxyhalides: modelling the properties of high Tc superconductors", *Faraday Discuss.*, **106**, 367.

[9] Islam, M. S. and Winch, L. J. (1995). "Defect chemistry and oxygen diffusion in the $HgBa_2Ca_2Cu_3O_{8+x}$ superconductor: a computer simulation study", *Phys. Rev. B*, **52**, 10510.

[10] Catlow, C. R. A. (1987). "Computational techniques and simulation of crystal structures" in Solid State Chemistry: Techniques, Eds., Cheetham, A. K. and Day, P., Clarendon Press, Oxford.

[11] Smith, W. and Forester, T. R. (1996). "DL_POLY 2.0: A general purpose parallel molecular dynamics simulation package", *J. Molec. Graphics*, **14**, 136.

[12] Ishigaki, T., Yamauchi, S., Kishio, K., Mizusaki, J. and Fueki, K. (1988). "Diffusion of oxide ion vacancies in perovskite-type oxides", *J. Solid State Chem.*, **73**, 179.

[13] Mizusaki, J. (1992). "Nonstoichiometry, diffusion and electrical properties of perovskite-type oxide electrode materials", *Solid State Ionics*, **52**, 79.

[14] Carter, S., Selcuk, A., Chater, R. J., Kajda, J., Kilner, J. A. and Steele, B. C. H. (1992). "Oxygen transport in selected nonstoichiometric perovskite-structure oxides", *Solid State Ionics*, **53–56**, 597.

[15] Belzner, A., Gur, T. M. and Huggins, R. A. (1992). "Oxygen chemical diffusion in strontium doped lanthanum manganites", *Solid State Ionics*, **57**, 327.

[16] Alcock, C. B., Doshi, R. C. and Shen, Y. (1992). "Perovskite electrodes for sensors", *Solid State Ionics*, **51**, 281.

[17] Yasuda, I. and Hishinuma, M. (1996). "Electrical conductivity and chemical diffusion coefficient of Sr-doped lanthanum manganites", *J. Solid State Chem.*, **123**, 382.

[18] Kharton, V. V., Naumovich, E. N., Vecher, A. A. and Nikolaev, A. V. (1995). "Oxide ion conduction in solid solutions $Ln_{1-x}Sr_xCoO_{3-x}$ (Ln = La, Pr, Nd)", *J. Solid State Chem.*, **120**, 128.

[19] ten Elshof, J. E., Bouwmeester, H. J. M. and Verweij, H. (1996). "Oxygen transport through $La_{1-x}Sr_xFeO_{3-y}$ membranes", *Solid State Ionics*, **89**, 81.

[20] van Doorn, R. H. E., Fullarton, I. C., de Souza, R. A., Kilner, J. A., Bouwmeester, H. J. M. and Burgraaf, A. J. (1997). "Surface oxygen exchange of $La_{0.3}Sr_{0.7}CoO_{3-x}$", *Solid State Ionics*, **96**, 1.

[21] Ishihara, T., Kilner, J. A., Honda, M. and Takita, T. (1997). "Oxygen surface exchange and diffusion in the new perovskite oxide ion conductor $LaGaO_3$", *J. Am. Chem Soc.*, **119**, 2747.

[22] Drennan, J., Zelizko, V., Hay, D., Ciacchi, F. T., Rajendren, S. and Badwal, S. P. S. (1997). 'Characterisation, conductivity and mechanical properties of the oxygen-ion conductor $La_{0.9}Sr_{0.1}Ga_{0.8}Mg_{0.2}O_{3-x}$", *J. Mater. Chem.*, **7**, 79.

[23] Benson, S. J., Chater, R. J. and Kilner, J. A. (1997). "Oxygen diffusion and surface exchange in the mixed conducting perovskite $La_{0.6}Sr_{0.4}Fe_{0.8}Co_{0.2}O_{3-\delta}$", in press.

[24] Cook, R. L. and Sammells, A. F. (1991). "On the systematic selection of perovskite solid electrolytes for intermediate temperature fuel cells", *Solid State Ionics*, **45**, 311.
[25] van Doorn, R. H. E., Bouwmeester, H. J. M. and Burgraaf, A. J., to be published.
[26] Li, X. and Hafskjold, B. (1995). "Molecular Dynamics simulations of yttrium-stabilized zirconia", *J. Phys. Condens. Matter*, **7**, 1255.